Acta Pharmaceutica Sinica B 2024;14(3):1241−1256

Chinese Pharmaceutical Association
Institute of Materia Medica, Chinese Academy of Medical Sciences

Acta Pharmaceutica Sinica B

www.elsevier.com/locate/apsb
www.sciencedirect.com

ORIGINAL ARTICLE

# Sulfation of chondroitin and bile acids converges to antagonize Wnt/β-catenin signaling and inhibit APC deficiency-induced gut tumorigenesis

**Pengfei Xu[a,b,*,†], Yue Xi[a,†], Jong-Won Kim[a], Junjie Zhu[a], Min Zhang[a], Meishu Xu[a], Songrong Ren[a], Da Yang[a], Xiaochao Ma[a], Wen Xie[a,c,*]**

[a]*Center for Pharmacogenetics and Department of Pharmaceutical Sciences, University of Pittsburgh, Pittsburgh, PA 15261, USA*
[b]*Department of Hepatobiliary and Pancreatic Surgery, Zhongnan Hospital of Wuhan University, School of Pharmaceutical Sciences, Wuhan University, Wuhan 430071, China*
[c]*Department of Pharmacology & Chemical Biology, University of Pittsburgh, Pittsburgh, PA 15261, USA*

Received 26 June 2023; received in revised form 6 October 2023; accepted 23 November 2023

**KEY WORDS**

Colon cancer;
APC;
Wnt/β-catenin;
PAPSS2;
Chondroitin sulfate;
Sulfation;
Bile acids;
FXR

**Abstract** Sulfation is a crucial and prevalent conjugation reaction involved in cellular processes and mammalian physiology. 3′-Phosphoadenosine 5′-phosphosulfate (PAPS) synthase 2 (PAPSS2) is the primary enzyme to generate the universal sulfonate donor PAPS. The involvement of PAPSS2-mediated sulfation in adenomatous polyposis coli (APC) mutation-promoted colonic carcinogenesis has not been reported. Here, we showed that the expression of PAPSS2 was decreased in human colon tumors along with cancer stages, and the lower expression of PAPSS2 was correlated with poor prognosis in advanced colon cancer. Gut epithelial-specific heterozygous *Apc* deficient and *Papss2*-knockout ($Apc^{\Delta gut\text{-}Het}Papss2^{\Delta gut}$) mice were created, and the phenotypes were compared to the spontaneous intestinal tumorigenesis of $Apc^{\Delta gut\text{-}Het}$ mice. $Apc^{\Delta gut\text{-}Het}Papss2^{\Delta gut}$ mice were more sensitive to gut tumorigenesis, which was mechanistically accounted for by the activation of Wnt/β-catenin signaling pathway due to the suppression of chondroitin sulfation and inhibition of the farnesoid X receptor

*Corresponding authors.
E-mail addresses: pengfeixu@whu.edu.cn (Pengfei Xu), wex6@pitt.edu (Wen Xie).
†These authors made equal contributions to this work.
Peer review under the responsibility of Chinese Pharmaceutical Association and Institute of Materia Medica, Chinese Academy of Medical Sciences.

https://doi.org/10.1016/j.apsb.2023.12.006

(FXR)-transducin-like enhancer of split 3 (TLE3) gene regulatory axis. Chondroitin sulfate supplementation in $Apc^{\Delta gut\text{-}Het}Papss2^{\Delta gut}$ mice alleviated intestinal tumorigenesis. In summary, we have uncovered the protective role of PAPSS2-mediated chondroitin sulfation and bile acids−FXR−TLE3 activation in the prevention of gut carcinogenesis *via* the antagonization of Wnt/$\beta$-catenin signaling. Chondroitin sulfate may be explored as a therapeutic agent for Papss2 deficiency-associated colonic carcinogenesis.



## 1. Introduction

Colorectal cancer (CRC) is the third most common malignancy and the second most deadly cancer, with an estimated 1.93 million new cases and 0.94 million deaths in 2020 worldwide[1]. Both the incidence and death of CRC are rising among young people. The United States and China have the highest predicted number of new CRC cases in the next several decades[2,3]. Multiple carcinogenic events, including serrated adenomas, adenoma-carcinoma sequence, and inflammation, contribute to the development of CRC[4,5]. The initiation of sporadic CRC is largely attributed to acquired somatic genetic mutations or epigenetic alterations induced by modifiable risk factors[6–9]. It is necessary to identify novel genes involved in the pathogenesis of CRC in order to develop effective treatments.

More than 80% of sporadic CRC patients have mutations in the tumor suppressor gene APC, which is an essential negative regulator of Wnt/$\beta$-catenin signaling[10]. APC blocks the Wnt signaling pathway by attaching to and promoting the degradation of $\beta$-catenin[11]. Mutations in the APC gene lead to loss of $\beta$-catenin regulation, altered cell migration and chromosome instability, and causing familial adenomatous polyposis (FAP) characterized by extensive intestinal polyp formation and a high risk of CRC development[12]. Mice with mutation of the Apc gene, such as the gut epithelial-specific heterozygous Apc deficient ($Apc^{\Delta gut\text{-}Het}$) mice, are commonly used to mimic human FAP and intestinal neoplasia in colon cancer-associated studies[13,14].

Sulfation is a vital biological process that modifies endogenous and exogenous chemicals as well as protein peptides in mammals. The 3′-phosphoadenosine 5′-phosphosulfate (PAPS) synthase 2 (PAPSS2) is the key enzyme to generate PAPS, which is synthesized from inorganic sulfate and ATP, and it is the universal sulfonate donor for all sulfation reactions[15]. We recently reported that intestinal ablation of Papss2 sensitized mice to the dextran sulfate sodium (DSS) model of colitis and colitis-associated carcinogenesis through the inhibition of mucin sulfation and compromised gut barrier function but without a defined molecular mechanism[16]. It is also unclear whether PAPSS2 also plays a role in colitis-independent colonic carcinogenesis, such as that induced by APC deficiency.

In this study, we found that intestinal ablation of Papss2 sensitized mice to the APC deficiency model of gut carcinogenesis. Mechanistically, compromised chondroitin sulfation and accumulation of FXR antagonistic bile acid species converge on the activation of Wnt/$\beta$-catenin signaling and sensitization of gut carcinogenesis.

## 2. Materials and methods

### 2.1. Human patient datasets and human cohort and scRNA-seq analyses

Gene expression data, correlation analysis, and clinical features of cancer patients were analyzed from The Cancer Genome Atlas (TCGA), and Gene Expression Profiling Interactive Analysis website (http://gepia.cancer-pku.cn). Human normal colon and colon tumor tissues array were purchased from US Biomax (Derwood, MD) and used for H&E and immunohistochemical staining. For human intestine and colon scRNA-seq analyses, the normal human small intestine and colon dataset was derived from the Human Protein Atlas browser (https://www.proteinatlas.org) to identify cell clusters and *PAPSS2* gene expression in different cell lineages.

### 2.2. Experimental animal studies

$Apc^{fl/-}$ mice (Strain #:009045) and Villin-cre mice (Strain #:004586) were obtained from Jackson Laboratory. $Papss2^{fl/fl}$ mice in the C57BL/6 genetic background were custom-made and previously described[16]. $Papss2^{fl/fl}$ mice were crossed with Villin-cre mice to create gut-specific *Papss2* knockout mice ($Papss2^{\Delta gut}$) and then crossed with $Apc^{fl/-}$ mice to generate gut epithelial-specific heterozygous Apc deficiency and *Papss2*-knockout ($Apc^{\Delta gut\text{-}Het}Papss2^{\Delta gut}$) mice, the littermate $Apc^{\Delta gut\text{-}Het}$ were used as controls. Sixteen-week-old $Apc^{\Delta gut\text{-}Het}$ and $Apc^{\Delta gut\text{-}Het}Papss2^{\Delta gut}$ were analyzed for their spontaneous int estinal tumorigenesis. Chondroitin sulfate (CS, CAS 9007-28-7, Purity: ≥90%) was purchased from Santa Cruz. When necessary, CS (400 mg/kg in $H_2O$) or vehicle was orally gavaged daily from 8 weeks of age for 8 weeks. Azoxymethane (AOM) was purchased from Sigma−Aldrich (St. Louis, MO, USA). In the AOM model of gut carcinogenesis, 8-week-old male mice were intraperitoneally injected with AOM (10 mg/kg body weight) once a week for 6 weeks. The mice were maintained for another 5 months to induce spontaneous colonic carcinogenesis[17]. Mice were euthanized by $CO_2$ asphyxiation, and their serum samples, colons, and intestines were collected. Bile acid contents were measured by collecting tissues and serum from mice that had fasted for 4 h. The samples were collected and immediately frozen in dry ice, then stored at −80 °C for subsequent analyses. The use of mice was in accordance with the University of Pittsburgh Institutional Animal Care and Use Committee (protocol numbers: 19044749 and 22030802).

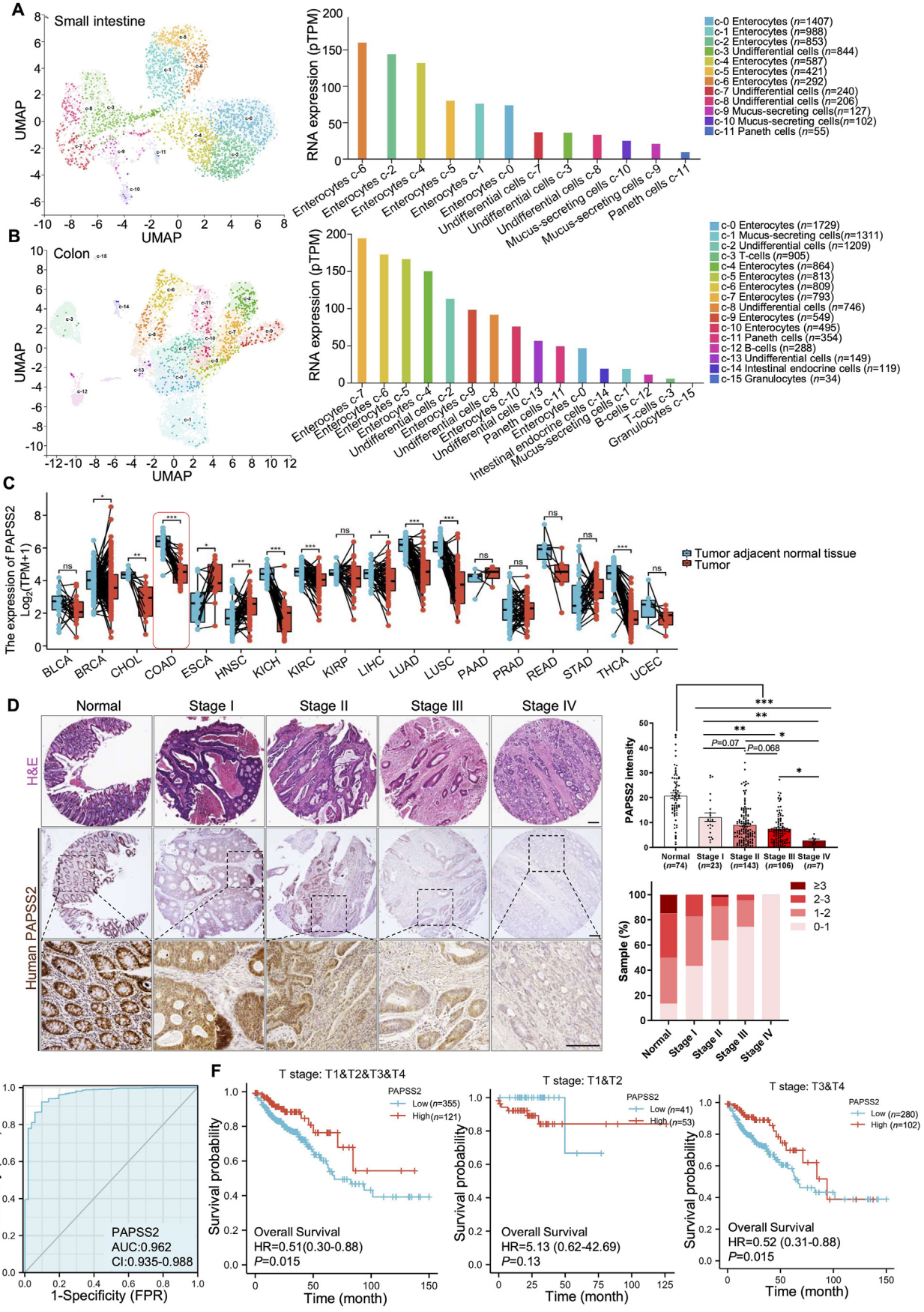
A
Small intestine
UMAP
RNA expression (pTPM)
c-0 Enterocytes (n=1407)
c-1 Enterocytes (n=988)
c-2 Enterocytes (n=853)
c-3 Undifferential cells (n=844)
c-4 Enterocytes (n=587)
c-5 Enterocytes (n=421)
c-6 Enterocytes (n=292)
c-7 Undifferential cells (n=240)
c-8 Undifferential cells (n=206)
c-9 Mucus-secreting cells(n=127)
c-10 Mucus-secreting cells(n=102)
c-11 Paneth cells (n=55)
Enterocytes c-6
Enterocytes c-2
Enterocytes c-4
Enterocytes c-5
Enterocytes c-1
Enterocytes c-0
Undifferential cells c-7
Undifferential cells c-3
Undifferential cells c-8
Mucus-secreting cells c-10
Mucus-secreting cells c-9
Paneth cells c-11
B
Colon
c-0 Enterocytes (n=1729)
c-1 Mucus-secreting cells(n=1311)
c-2 Undifferential cells (n=1209)
c-3 T-cells (n=905)
c-4 Enterocytes (n=864)
c-5 Enterocytes (n=813)
c-6 Enterocytes (n=809)
c-7 Enterocytes (n=793)
c-8 Undifferential cells (n=746)
c-9 Enterocytes (n=549)
c-10 Enterocytes (n=495)
c-11 Paneth cells (n=354)
c-12 B-cells (n=288)
c-13 Undifferential cells (n=149)
c-14 Intestinal endocrine cells (n=119)
c-15 Granulocytes (n=34)
Enterocytes c-7
Enterocytes c-6
Enterocytes c-5
Enterocytes c-4
Undifferential cells c-2
Enterocytes c-9
Undifferential cells c-8
Enterocytes c-10
Undifferential cells c-13
Paneth cells c-11
Enterocytes c-0
Intestinal endocrine cells c-14
Mucus-secreting cells c-1
B-cells c-12
T-cells c-3
Granulocytes c-15
C
The expression of PAPSS2 Log2(TPM+1)
Tumor adjacent normal tissue
Tumor
BLCA
BRCA
CHOL
COAD
ESCA
HNSC
KICH
KIRC
KIRP
LIHC
LUAD
LUSC
PAAD
PRAD
READ
STAD
THCA
UCEC
D
Normal
Stage I
Stage II
Stage III
Stage IV
H&E
Human PAPSS2
PAPSS2 intensity
P=0.07
P=0.068
Normal (n=74)
Stage I (n=23)
Stage II (n=143)
Stage III (n=106)
Stage IV (n=7)
Sample (%)
≥3
2-3
1-2
0-1
E
Sensitivity (TPR)
1-Specificity (FPR)
PAPSS2
AUC:0.962
CI:0.935-0.988
F
T stage: T1&T2&T3&T4
PAPSS2
Low (n=355)
High (n=121)
Survival probability
Overall Survival
HR=0.51(0.30-0.88)
P=0.015
Time (month)
T stage: T1&T2
Low (n=41)
High (n=53)
Overall Survival
HR=5.13 (0.62-42.69)
P=0.13
T stage: T3&T4
Low (n=280)
High (n=102)
Overall Survival
HR=0.52 (0.31-0.88)
P=0.015

### 2.3. Immunostaining and Western blot analysis

Deparaffinization and rehydration were performed on paraffin sections. Antibodies against $\beta$-catenin (Cell Signaling Technology, #8480), chondroitin sulfate (Abcam, ab11570), and Ki67 (Abcam, ab15580) were used for immunofluorescence (IF). PAPSS2 (Santa Cruz, sc-100801) and TLE3 (Proteintech, 11372-1-AP) antibodies were used for immunohistochemistry and incubated at 4 °C overnight. The appropriate fluorescent secondary antibodies or the VECTASTAIN ABC Kit were used, and DAB Peroxidase Substrate Kit from Vector Laboratories was used for visualizing the staining. The percentage of positive area per mouse was determined by calculating the quantifications of the positive area from immunostaining using Image J software. For Western blot analysis, tissue protein samples were extracted using radioimmunoprecipitation assay buffer containing a protease inhibitor cocktail. Western blotting was conducted as previously described[18,19]. The membranes were incubated with primary antibodies against $\beta$-actin (Sigma, A1978), $\beta$-catenin (Cell Signaling Technology, #8480), chondroitin sulfate (Abcam, ab11570), PAPSS2 (Santa Cruz, sc-100801), and TLE3 (Proteintech, 11372-1-AP) followed by appropriate secondary antibodies.

### 2.4. Isolation and culture of mouse intestinal organoids

Intestinal crypts were isolated and cultured following a previously described protocol with minor adjustments[16]. In brief, the ileums were first washed in ice-cold PBS, and then sliced into 1−2 mm fragments, which were washed 15−20 times in PBS to eliminate any impurities. Next, Gentle Cell Dissociation Reagent (GCDR, cat #7174, Stem cell technologies, MA, USA) was applied in accordance with the manufacturer's instructions. To culture intestinal organoids, the crypts were tallied and then embedded in Matrigel, and maintained in IntestiCult organoid growth medium (cat #6005, Stem cell technologies, MA, USA). When applicable, $NaClO_3$ (Sigma, 403016, 50 mmol/L), cardamonin (MedChemExpress, HY-N0279, 10 μmol/L), or chondroitin sulfate (CS) (MedChemExpress, HY-B2162, Purity: ≥95.0%, 500 μg/mL, 1000 μg/mL) were added into the culture medium from the 1st day to the 6th day with the medium changed every two days.

### 2.5. RNA-seq data analysis

The RNeasy Mini Kit was used to extract total RNA, which was then subjected to library preparation. RNA-seq was conducted at the Health Sciences Sequencing Core at the Children's Hospital of Pittsburgh, and the results were analyzed as we previously described[20].

### 2.6. Macroscopic and histological analysis

The gut tumor area and number were determined in whole-mount tissue. The colon and intestine tissues were flushed with phosphate-buffered saline (PBS) and then fixed overnight in 10% formalin. After paraffin embedding, 4−5 μm tissue sections were prepared using a microtome. The sections were then deparaffinized, rehydrated, and subjected to histological analysis using H&E staining and immunostaining as previously reported[16]. The positive staining area was quantified using ImageJ software.

### 2.7. Plasmid construction, cell transfection, and luciferase reporter gene assays

The human pCDNA-PAPSS2 expression vector was cloned using standard molecular cloning techniques. All cloned sequences were verified by DNA sequencing at the University of Pittsburgh Genomics Research Core. The T-cell factor/lymphoid enhancer factor (TCF/LEF) luciferase reporter plasmid was obtained from Addgene (Watertown, MA, USA). The GAL4-hFXR and tk-UAS luciferase reporter plasmids were from our lab. HCT116 cells were used for transfection and luciferase reporter gene assay. Cells were transfected with plasmids using Lipofectamine 3000 from Thermo Fisher Scientific (Carlsbad, CA, USA). When applicable, transfected cells were treated with $NaClO_3$ (25 and 50 mmol/L), Tauro-$\beta$-muricholic acid (T$\beta$MCA, 50 μmol/L), fexaramine (Fex, 50 μmol/L), CS (500 and 1000 μg/mL), cholic acid (CA, 20 μmol/L), CA-sulfate (20 μmol/L), taurocholic acid (TCA, 20 μmol/L), or TCA-sulfate (20 μmol/L) for 24 h before cell harvesting. Luciferase activity was measured and normalized against $\beta$-gal activity from the co-transfected pCMX-$\beta$-gal.

### 2.8. Cytokine and cancer tumor marker measurement

For cytokine measurements, serum or tissue lysates were collected and the levels of Interleukin 1$\beta$ (IL-1$\beta$), or tumor necrosis factor alpha (TNF$\alpha$) were determined using enzyme-linked immunosorbent assay (ELISA) kits from R&D Systems (Minneapolis, MN, USA). Carcinoembryonic Antigen (CEA) ELISA Kit was obtained from LSbio (Shirley, MA, USA). Tissue lysates were prepared by homogenizing tissues in lysis buffer containing a protease inhibitor cocktail.

**Figure 1** Decreased expression of PAPSS2 correlates with poor survival of colon cancer patients. (A, B) Bioinformatic analyses of scRNA-seq dataset derived from normal human gut. Shown are scaled expression of *PAPSS2* in different cell lineages and clustering of different cell lineages in small intestine (A) and colon (B). (C) Analysis of *PAPSS2* gene expression in paired tumor adjacent normal tissues and primary tumors in TCGA cohorts of cancers. BLCA, bladder urothelial carcinoma; BRCA, breast invasive carcinoma; CHOL, cholangiocarcinoma; COAD, colon adenocarcinoma (red box); ESCA, esophageal carcinoma; HNSC, head and neck squamous cell carcinoma; KICH, kidney chromophobe; KIRC, kidney renal clear cell carcinoma; KIRP, kidney renal papillary cell carcinoma; LIHC, liver hepatocellular carcinoma; LUAD, lung adenocarcinoma; LUSC, lung squamous cell carcinoma; PAAD, pancreatic adenocarcinoma; PRAD, prostate adenocarcinoma; READ, rectum adenocarcinoma; STAD, stomach adenocarcinoma; THCA, thyroid carcinoma; UCEC, uterine corpus endometrial carcinoma. (D) Representative H&E and IHC staining of PAPSS2 on human normal colon and different stages of colon cancer tissue array. Shown on the right is the quantifications of PAPSS2 positive area. Scale bars: 100 μm. (E) Receiver operating characteristic (ROC) curve analysis for PAPSS2 as a predictor of patients with colon cancer. (F) Parsing of human COAD patient survival curves in different stages based on the *PAPSS2* expression. One-way ANOVA with Tukey's test was used for multiple comparisons. Survival curves were plotted using the Kaplan−Meier method, and the log-rank test was utilized to determine statistical differences. Data are presented as the mean ± SEM. ns means no significant difference; $^{*}P < 0.05$; $^{**}P < 0.01$; $^{***}P < 0.001$.

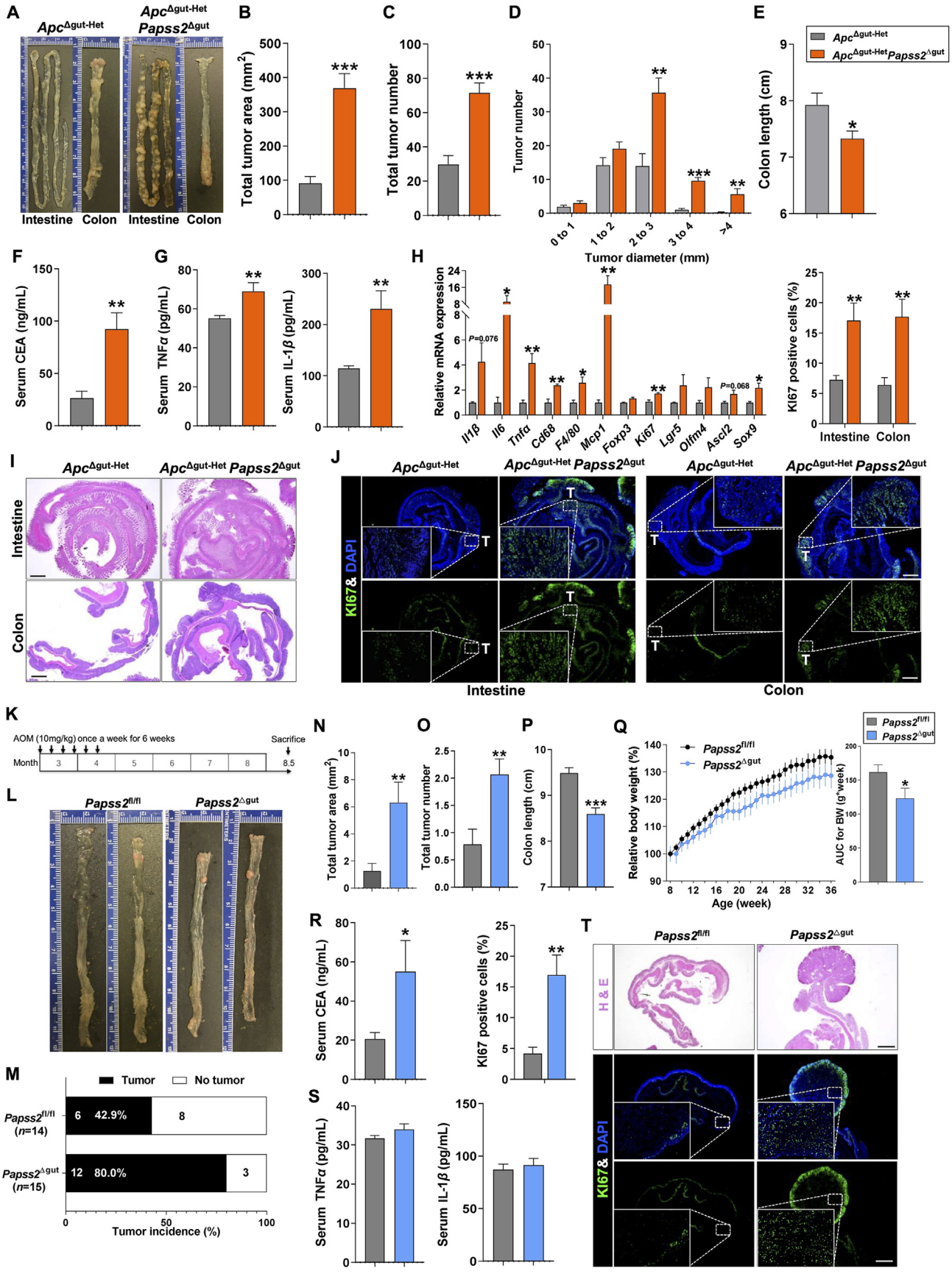
A
Apc^Δgut-Het
Apc^Δgut-Het Papss2^Δgut
Intestine Colon Intestine Colon
B
Total tumor area (mm²)
C
Total tumor number
D
Tumor number
0 to 1
1 to 2
2 to 3
3 to 4
>4
Tumor diameter (mm)
E
Apc^Δgut-Het
Apc^Δgut-Het Papss2^Δgut
Colon length (cm)
F
Serum CEA (ng/mL)
G
Serum TNFα (pg/mL)
Serum IL-1β (pg/mL)
H
Relative mRNA expression
P=0.076
P=0.068
Il1β Il6 Tnfα Cd68 F4/80 Mcp1 Foxp3 Ki67 Lgr5 Olfm4 Ascl2 Sox9
Ki67 positive cells (%)
Intestine Colon
I
Apc^Δgut-Het
Apc^Δgut-Het Papss2^Δgut
Intestine
Colon
J
Apc^Δgut-Het
Apc^Δgut-Het Papss2^Δgut
Ki67& DAPI
T
Intestine
Colon
K
AOM (10mg/kg) once a week for 6 weeks
Sacrifice
Month 3 4 5 6 7 8 8.5
L
Papss2^fl/fl
Papss2^Δgut
M
Tumor
No tumor
Papss2^fl/fl (n=14)
6 42.9%
8
Papss2^Δgut (n=15)
12 80.0%
3
Tumor incidence (%)
N
Total tumor area (mm²)
O
Total tumor number
P
Colon length (cm)
Q
Papss2^fl/fl
Papss2^Δgut
Relative body weight (%)
Age (week)
AUC for BW (g*week)
R
Serum CEA (ng/mL)
Ki67 positive cells (%)
S
Serum TNFα (pg/mL)
Serum IL-1β (pg/mL)
T
Papss2^fl/fl
Papss2^Δgut
H & E
Ki67& DAPI

### 2.9. Bile acids quantification

Total bile acids from serum and ileal lysates were measured using an assay kit from Biovision (Milpitas, CA, USA). For bile acid species profiling, ileal tissues were homogenized in water (100 mg tissue in 400 μL water), and then added twice the volume of methanol/acetonitrile (1:1). After two rounds of vortexing for 1 min each, the mixture was centrifuged at 15,000 × *g* for 20 min, and 2 μL of the supernatants were injected into the ultra-performance liquid chromatography and quadrupole time-of-flight mass spectrometry (UPLC−QTOFMS) system for analysis. Bile acid analysis was conducted using an Acquity UPLC BEH C18 column (2.1 mm × 100 mm, 1.7 μm) as previously described[21]. Bile acid sulfates were analyzed using an Acquity UPLC HSS T3 column (2.1 mm × 100 mm, 1.8 μm) with a mobile phase of acetonitrile/water containing 10 mmol/L ammonium acetate. The mass parameters were detailed in a previous report[22].

### 2.10. Quantitative real-time PCR

RNA extraction was performed using the Trizol reagent from Invitrogen (Carlsbad, CA, USA). Two μg of total RNA were used for cDNA synthesis with a reverse transcription kit from Thermo Fisher Scientific (Waltham, MA, USA). Real-time PCR was carried out using SYBR Green reagent on the QuantStudioTM 6 Flex Real-Time PCR System from Applied Biosystems, as previously described[23]. The comparative ΔΔCT method was used for data analysis, and Cyclophilin or *Gapdh* were used as housekeeping gene controls. The primer sequences used are listed in Supporting Information Table S1.

### 2.11. Statistical analysis

The statistical analysis was conducted using Prism GraphPad 9.0 software (San Diego, CA, USA). Experimental data are presented as means ± standard error of mean (SEM) or box plots. Statistical significance between two groups was assessed by two-tailed Student's *t*-test. One-way ANOVA with Tukey's test was used for multiple comparisons. Survival curves were plotted using the Kaplan−Meier method, and the log-rank test was utilized to determine statistical differences. The gene expression correlation analysis was performed using the Pearson correlation coefficient. A significance level of $P < 0.05$ was considered statistically significant.

## 3. Results

### 3.1. Decreased expression of PAPSS2 correlates with poor clinical outcome of colon cancer patients

To understand the role of PAPSS2-mediated sulfation in human pathophysiology, we analyzed *PAPSS2* mRNA and protein expression in various human tissues based on several datasets in the Human Protein Altas[24]. PAPSS2 was found to be highly expressed in the human gut system (Supporting Information Fig. S1A−S1D). The gut is an organ of multiple cell types. To define the cellular source of PAPSS2, we analyzed a publicly available scRNA-seq dataset derived from normal human gut (https://www.proteinatlas.org)[25] and found that among cell clusters, enterocytes, also known as simple columnar epithelial cells, had the highest expression of PAPSS2 in both the small intestine (Fig. 1A) and colon (Fig. 1B).

To further determine the role of PAPSS2 in human cancers, we analyzed the TCGA database and found that the expression of *PAPSS2* was decreased in 9 out of 18 paired cancer types (Fig. 1C), and in 15 out of 33 unpaired cancer types (Supporting Information Fig. S2A), including colon cancer. The decreased expression of PAPSS2 in human colon tumors was validated by immunohistochemistry analysis of colon cancer tissue array that included 74 normal colon tissues and 279 colon tumors, with the most marked suppression in advanced colon cancer (Fig. 1D). The receiver operator characteristic (ROC) curves, based on the analysis of PAPSS2 expression in colon adenocarcinoma (COAD) patients, indicated that PAPSS2 expression had a discriminatory power to distinguish COAD patients from patients without COAD with an optimism-corrected AUC of 0.962 (Fig. 1E).

In understanding the clinical relevance of decreased expression of PAPSS2 in cancers, we found that the lower expression of PAPSS2 was strongly correlated with poorer survival in the TCGA cohorts of five cancer types, including COAD, head and neck squamous cell carcinoma (HNSC), pancreatic adenocarcinoma (PAAD), kidney renal clear cell carcinoma (KIRC), and lung adenocarcinoma (LUAD) (Fig. S2B). A comparison of 476 patients with COAD from the TCGA database with tumor stages from T1 to T4 showed that the overall lower expression of PAPSS2 was significantly associated with poorer prognosis, with the most obvious correlation in advanced T3 and T4 stages (Fig. 1F). These results suggested that PAPSS2 may play a critical role in intestinal tumorigenesis.

### 3.2. Intestinal ablation of Papss2 sensitizes mice to APC-model of gut tumorigenesis

The gut epithelial-specific heterozygous *Apc* deficient mice represent a well-established model of gut tumorigenesis[11]. To determine whether inhibition of PAPSS2 plays a pathogenic role in colon cancer, we generated $Apc^{\Delta gut\text{-}Het}Papss2^{\Delta gut}$ mice by crossbreeding the floxed $Papss2^{fl/fl}$ mice[26] with the gut epithelial specific Villin-Cre transgenic mice and heterozygous floxed $Apc^{fl/-}$ mice, as outlined in Supporting Information Fig. S3A and S3B. The $Apc^{\Delta gut\text{-}Het}$ and $Apc^{\Delta gut\text{-}Het}Papss2^{\Delta gut}$ mice were genotyped by PCR (Fig. S3C). The efficiency of *Papss2* mRNA knockout in the small intestine and colon, but not in the liver, of

**Figure 2** Intestinal ablation of *Papss2* sensitizes mice to gut tumorigenesis. (A)−(J) $Apc^{\Delta gut\text{-}Het}$ and $Apc^{\Delta gut\text{-}Het}Papss2^{\Delta gut}$ mice were sacrificed and evaluated for spontaneous gut tumorigenesis when they were at 16 weeks of age ($n = 10$). Shown are representative gross appearance of the intestines and colons (A), total tumor area (B), total tumor number (C), tumor size distribution (D), colon length (E), serum levels of CEA (F) and TNFα and IL-1β (G), relative expression of ileal inflammatory and intestinal/cancer stem cell marker genes (H), and representative H&E (I) and immunofluorescence of Ki67 (J, green, with the quantifications shown on the upper right) in intestine and colon sections ($n = 5$). Scale bars: 1 mm. (K)−(T) Eight-week-old male $Papss2^{fl/fl}$ and $Papss2^{\Delta gut}$ mice were subjected to the AOM alone model of colon cancer for 6.5 months. $n = 14$−15. Shown are the scheme of 8-week-old mice treated with 6 rounds of AOM for 6.5 months to induce colon cancer (K), representative gross appearance of the colons (L), prevalence of tumor incidence (M), total tumor area (N), total tumor number (O), colon length (P), relative body weight and AUC of body weight (Q), serum levels of CEA (R) and TNFα and IL-1β (S), and representative H&E and immunofluorescence of Ki67 (green, with the quantifications shown on the top left) in colon sections (T). Scale bars: 1 mm. Statistical significance between two groups was assessed by two-tailed Student's *t*-test. Data are presented as the mean ± SEM. *$P < 0.05$; **$P < 0.01$; ***$P < 0.001$.

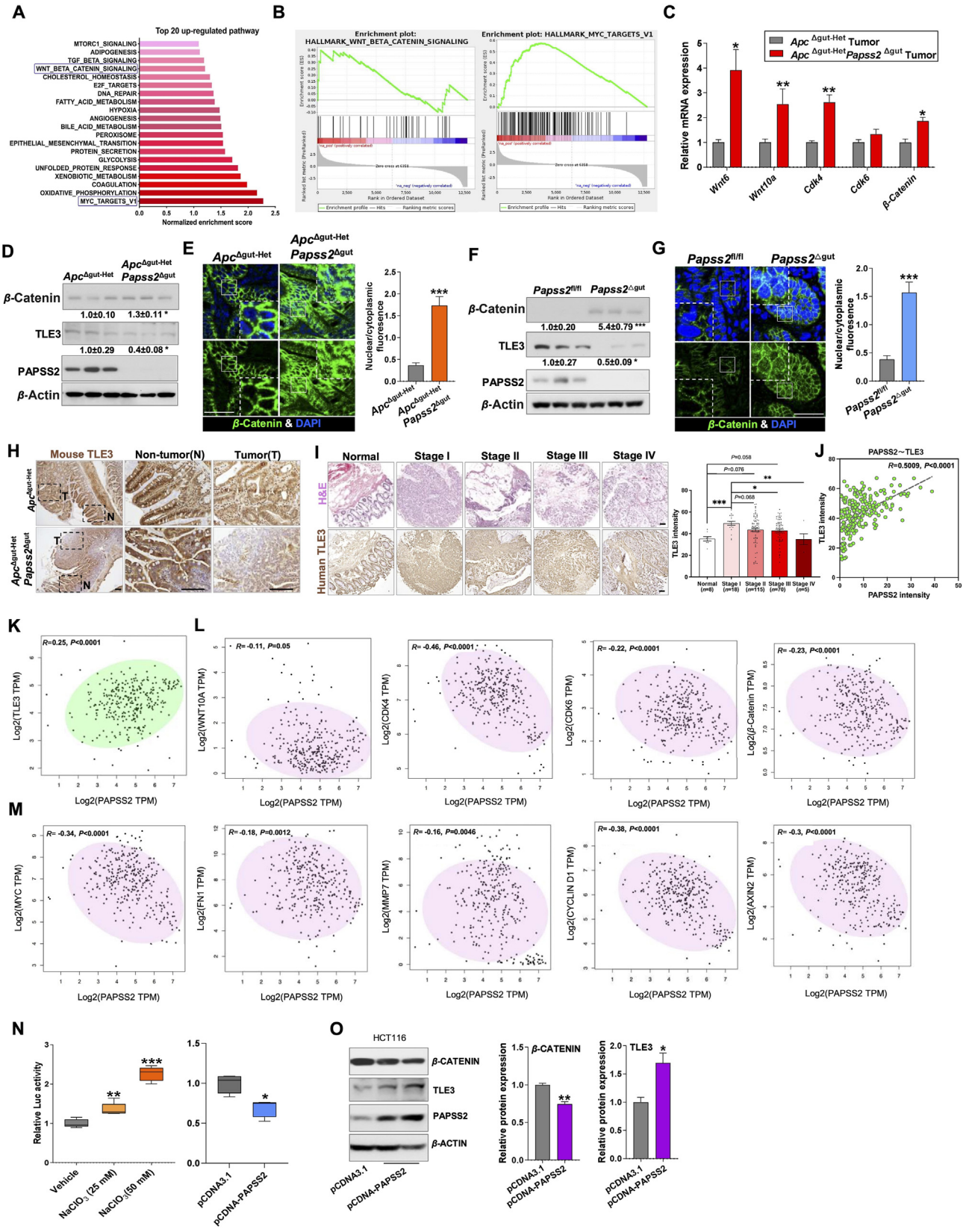


**Figure 3** Sensitization of gut tumorigenesis by intestinal *Papss2* ablation is accompanied by the activation of Wnt/β-catenin and suppression of Wnt repressor TLE3. (A, B) Top 20 hallmark pathways (A) and GSEA (B) of RNA-seq data from the intestinal tumor of $Apc^{\Delta gut\text{-}Het}$ and $Apc^{\Delta gut\text{-}Het}Papss2^{\Delta gut}$ mice. (C) Relative mRNA expression of Wnt target genes. (D) Protein expression of β-catenin and TLE3 in the ileum by Western blotting. (E) Representative β-catenin immunostaining (green) of tumor sections with the quantifications of the nuclear-to-cytoplasmic ratio of β-catenin fluorescence shown on the right. $n = 5$, scale bars: 200 μm. (F) Protein expression of β-catenin and TLE3 in the colon of

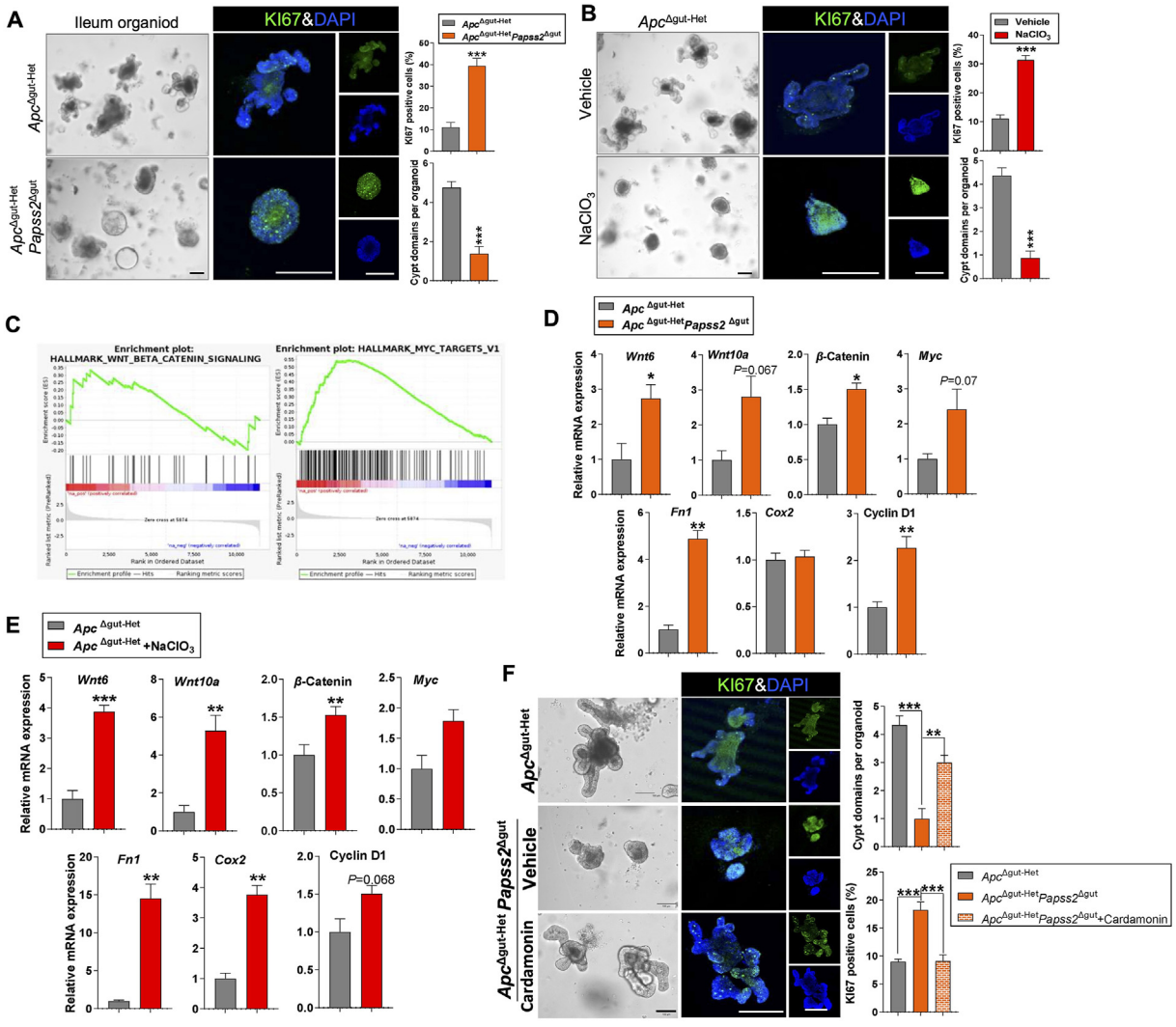


**Figure 4** Inhibition of PAPSS2 suppresses intestinal organoid differentiation and activates Wnt/β-catenin signaling. (A, B) Representative images and immunofluorescence of Ki67 of organoids isolated from the ileum of $Apc^{\Delta gut\text{-}Het}$ and $Apc^{\Delta gut\text{-}Het}Papss2^{\Delta gut}$ mice (A) or $Apc^{\Delta gut\text{-}Het}$ mice treatment with or without $NaClO_3$ (50 mmol/L) (B). $n = 5$, scale bars: 100 μm. Shown on the right are the quantifications of organoid differentiation and Ki67 signals. (C) GSEA of RNA-seq data from organoids isolated from the ileum of $Apc^{\Delta gut\text{-}Het}$ mice treatment with or without $NaClO_3$ (50 mmol/L). (D, E) Relative mRNA expression of Wnt target genes of organoid isolated from $Apc^{\Delta gut\text{-}Het}$ and $Apc^{\Delta gut\text{-}Het}Papss2^{\Delta gut}$ mice (D), or $Apc^{\Delta gut\text{-}Het}$ mice treatment with or without $NaClO_3$ (50 mmol/L) (E). (F) Representative images and Ki67 immunofluorescence of organoids isolated from the ileum of $Apc^{\Delta gut\text{-}Het}$ and $Apc^{\Delta gut\text{-}Het}Papss2^{\Delta gut}$ mice and treatment with or without Wnt/β-catenin inhibitor cardamonin (10 μmol/L). Shown on the right are the quantifications of organoid crypts and relative Ki67 signals. $n = 6$, scale bars: 100 μm. Statistical significance between two groups was assessed by two-tailed Student's *t*-test. Data are presented as the mean ± SEM. $^*P < 0.05$; $^{**}P < 0.01$; $^{***}P < 0.001$.

AOM-treated $Papss2^{fl/fl}$ and $Papss2^{\Delta gut}$ mice by Western blotting. (G) Representative β-catenin immunostaining (green) of colonic tumor with the quantifications of the nuclear-to-cytoplasmic ratio of β-catenin fluorescence shown on the right. $n = 5$, scale bars: 200 μm. (H) Representative TLE3 immunostaining in the tumor (T) or nontumor (N) regions of $Apc^{\Delta gut\text{-}Het}$ and $Apc^{\Delta gut\text{-}Het}Papss2^{\Delta gut}$ mice. Scale bars: 100 μm. (I) Representative H&E and IHC staining of TLE3 on human normal colon and different stages of colon cancer tissue array. Shown on the right is the quantifications of TLE3 positive area. Scale bars: 100 μm. (J) Correlations between the immunohistochemical intensity of PAPSS2 and TLE3 in the same cohort of samples shown in (I). (K−M) Correlations between the expression of PAPSS2 and TLE3 (K), Wnt target genes (L) and β-catenin target genes (M) in human COAD patient cohorts from TCGA using Gene Expression Profiling Interactive Analyses. (N) Luciferase reporter gene assay in HCT116 cells transfected with the TCF/TEF-luciferase reporter and treated with sulfation inhibitor $NaClO_3$ (left panel), or co-transfected with pCDNA-PAPSS2 expression plasmid (right panel). $n = 4$−5. (O) Protein expression of β-Catenin and TLE3 in the HCT116 cells transfected with pCDNA3.1 vector or pCDNA-PAPSS2. Shown on the right are the quantifications of protein expressions. $n = 3$−4. Statistical significance between two groups was assessed by two-tailed Student's *t*-test. One-way ANOVA with Tukey's test was used for multiple comparisons. The gene expression correlation analysis was performed using the Pearson correlation coefficient. Data are presented as the mean ± SEM or box plots. $^*P < 0.05$; $^{**}P < 0.01$; $^{***}P < 0.001$.

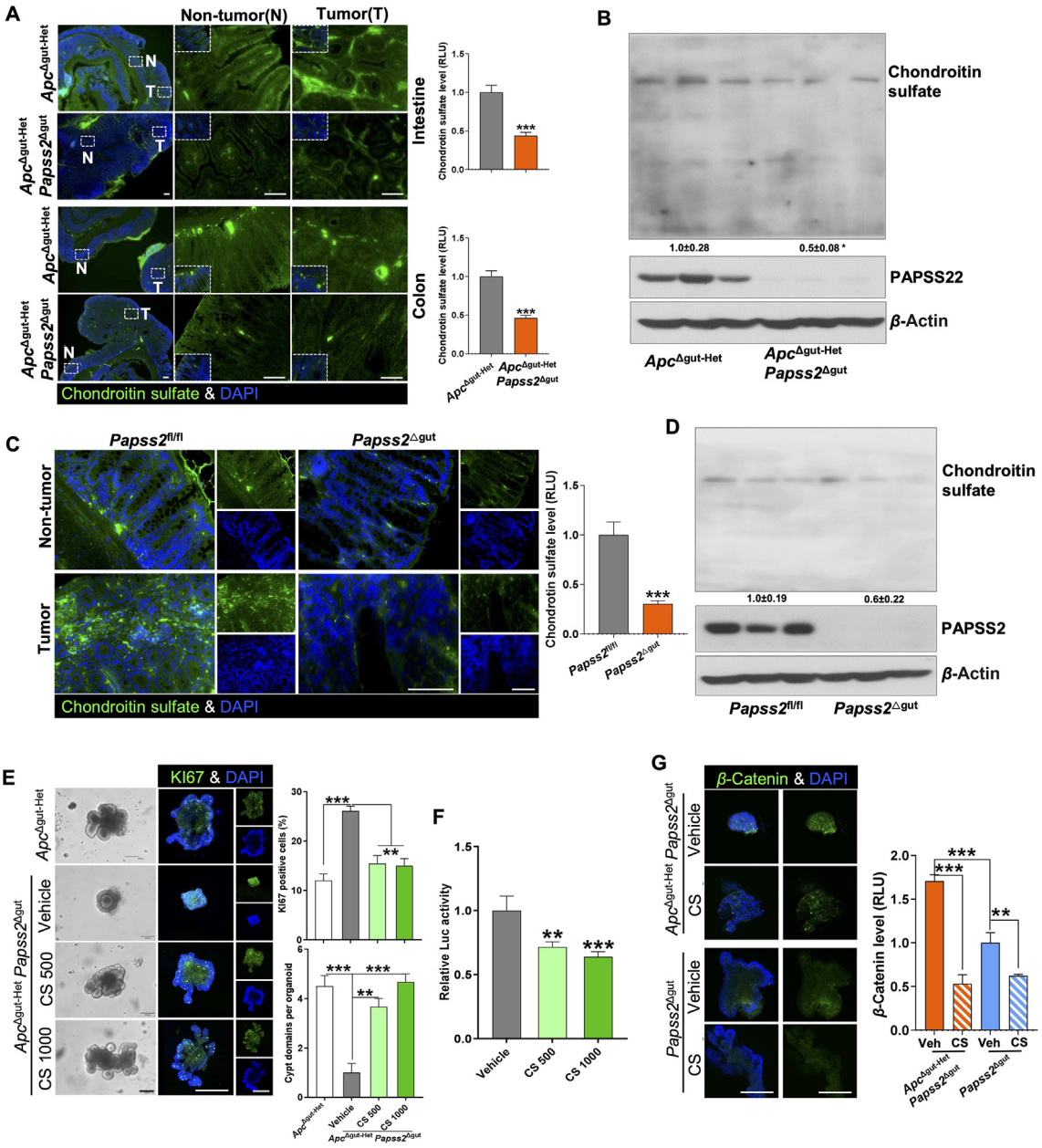


**Figure 5** Intestinal deficiency of *Papss2* inhibits chondroitin sulfation, leading to β-catenin activation. (A) Representative chondroitin sulfate immunostaining and quantifications of relative chondroitin sulfate levels in the intestine and colon tumor (T) or nontumor (N) regions of $Apc^{\Delta gut\text{-}Het}$ and $Apc^{\Delta gut\text{-}Het}Papss2^{\Delta gut}$ mice. $n = 5$, scale bars:100 μm. (B) Ileal level of chondroitin sulfate detected by Western blotting with the quantifications labeled. (C) Representative chondroitin sulfate immunostaining and quantifications of relative chondroitin sulfate levels in the colon tumor (T) or nontumor (N) regions of AOM-treated $Papss2^{fl/fl}$ and $Papss2^{\Delta gut}$ mice. $n = 5$, scale bars:100 μm. (D) Level of chondroitin sulfate detected by Western blotting with the quantifications labeled. (E) Representative appearance and Ki67 immunofluorescence of organoids isolated from the ileum of $Apc^{\Delta gut\text{-}Het}$ and $Apc^{\Delta gut\text{-}Het}Papss2^{\Delta gut}$ mice and treatment with indicated doses of chondroitin sulfate (CS, 500 and 1000 μg/mL). Shown on the right are the quantifications of organoid crypts and relative Ki67 signals. $n = 5–6$, scale bars: 100 μm. (F) Luciferase reporter assay in HCT116 cells transfected with TCF/TEF-luciferase reporter and treatment with CS for 24 h before cell harvesting and luciferase assay. $n = 4$. (G) Representative β-catenin immunofluorescence of organoids isolated from the ileum of $Apc^{\Delta gut\text{-}Het}Papss2^{\Delta gut}$ and AOM-treated $Papss2^{\Delta gut}$ mice and treatment without or with CS. Shown on the right are the quantifications of relative β-catenin signals. $n = 5$, scale bars: 100 μm. Statistical significance between two groups was assessed by two-tailed Student's *t*-test. One-way ANOVA with Tukey's test was used for multiple comparisons. Data are presented as the mean ± SEM. $^*P < 0.05$; $^{**}P < 0.01$; $^{***}P < 0.001$.

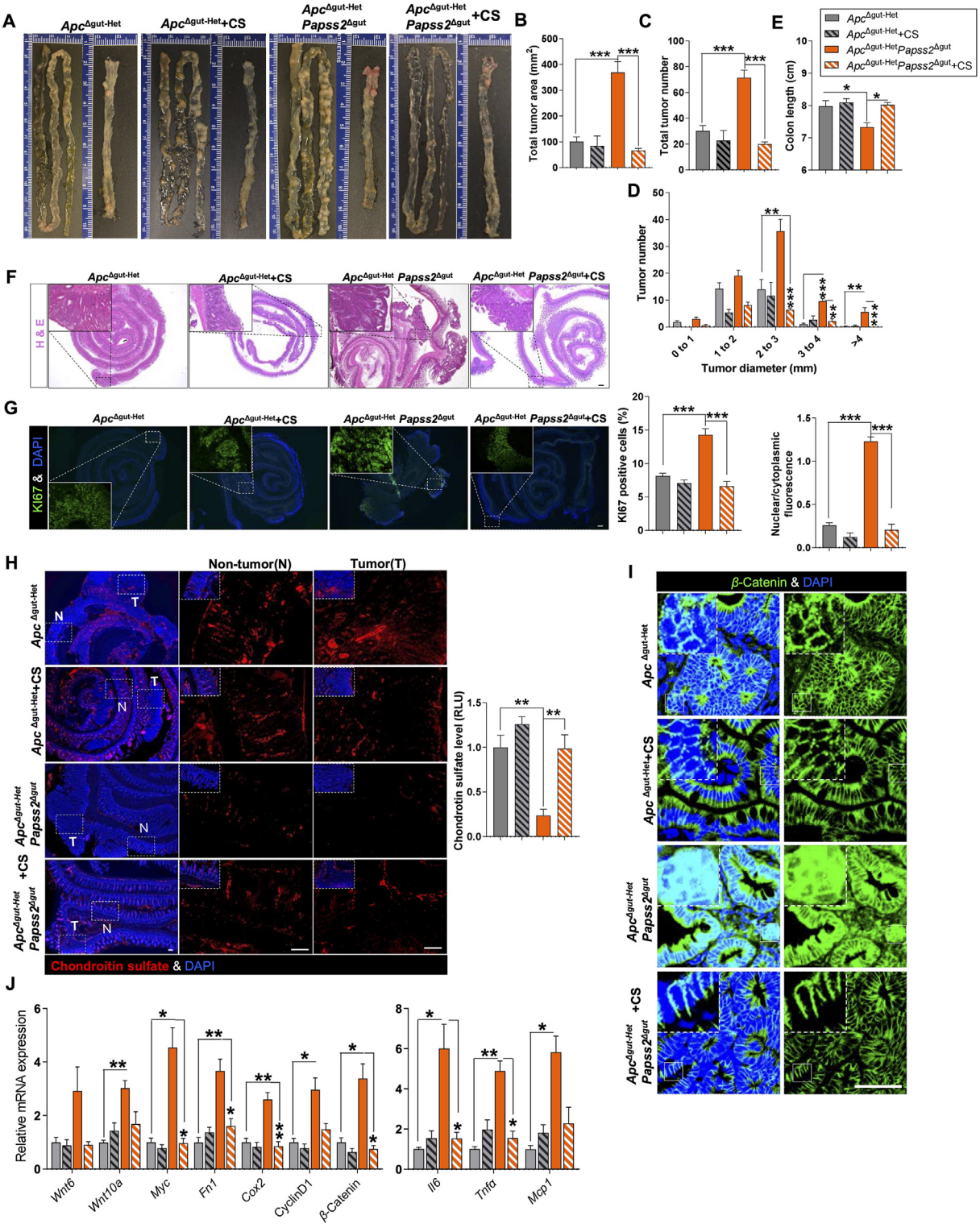


**Figure 6** Chondroitin sulfate supplementation attenuates gut tumorigenesis in Apc$^{\Delta gut\text{-}Het}$Papss2$^{\Delta gut}$ mice. Eight-week-old *Apc*$^{\Delta gut\text{-}Het}$ and *Apc*$^{\Delta gut\text{-}Het}$*Papss2*$^{\Delta gut}$ mice were monitored for spontaneous intestinal tumorigenesis with or without daily CS (400 mg/kg/day) gavage for 8 weeks. $n = 3-12$. (A) Representative gross appearance of the intestines and colons. (B) Total tumor area. (C) Total tumor number. (D) Tumor size distribution. (E) Colon length. (F) Representative H&E staining. Scale bars: 1 mm. (G) Representative immunofluorescence of Ki67 in intestinal sections and Ki67 with the quantifications shown on the right ($n = 5$). Scale bars: 1 mm. (H) Representative chondroitin sulfate immunostaining of intestine and colon tumor (T) or nontumor (N) regions with the quantifications shown on the right. $n = 5$, scale bars: 100 μm. (I) Representative β-catenin immunostaining of intestinal tumor with the quantifications of nuclear-to-cytoplasmic ratio of β-catenin fluorescence shown upper right. $n = 5$, scale bars: 50 μm. (J) Relative ileal mRNA levels of Wnt target genes and pro-inflammatory genes. $n = 3-5$. One-way ANOVA with Tukey's test was used for multiple comparisons. Data are presented as the mean ± SEM. $^*P < 0.05$; $^{**}P < 0.01$; $^{***}P < 0.001$.

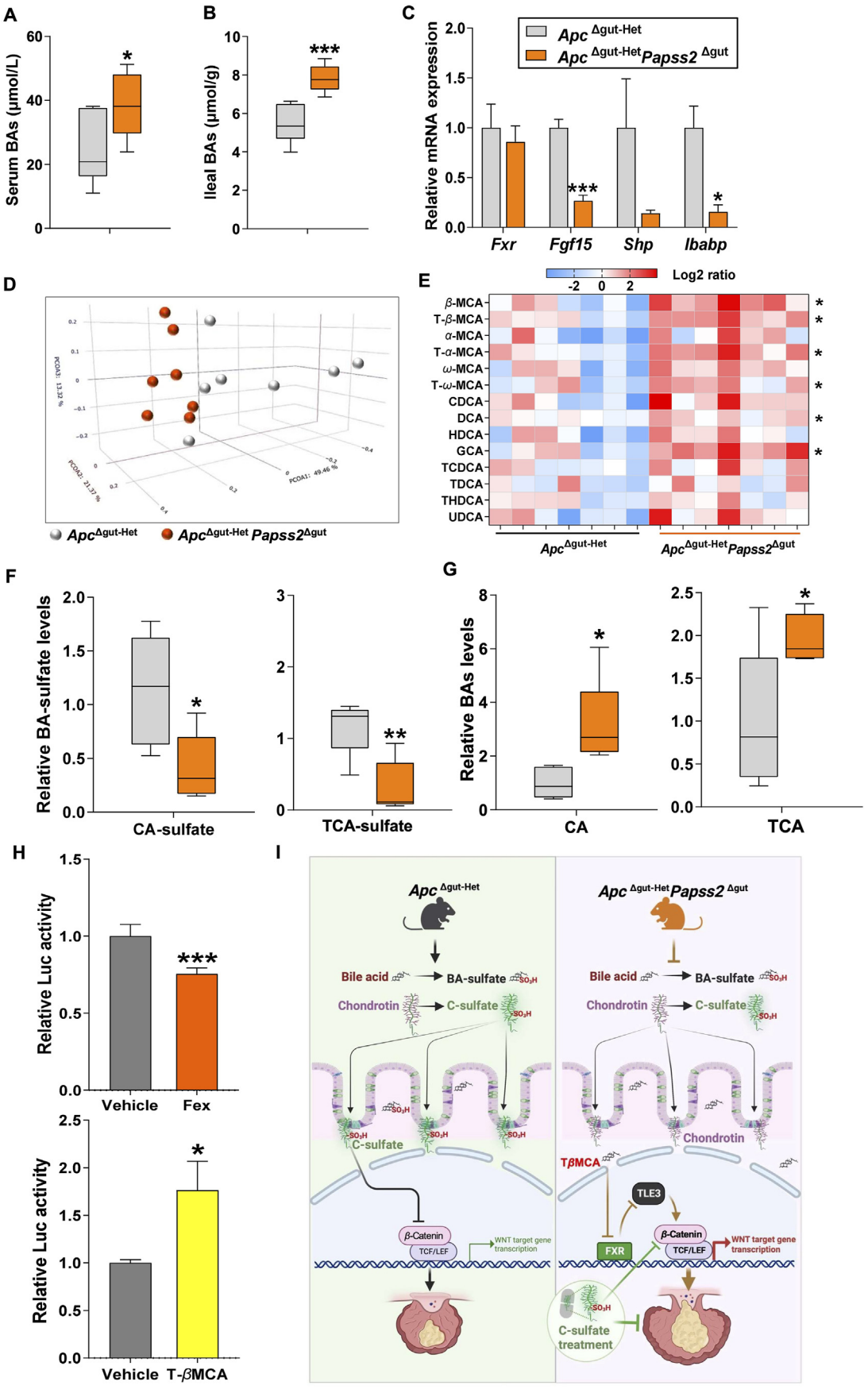
A
Serum BAs (μmol/L)
B
Ileal BAs (μmol/g)
C
Relative mRNA expression
Apc Δgut-Het
Apc Δgut-Het Papss2 Δgut
Fxr
Fgf15
Shp
Ibabp
D
Apc Δgut-Het
Apc Δgut-Het Papss2 Δgut
E
Log2 ratio
β-MCA
T-β-MCA
α-MCA
T-α-MCA
ω-MCA
T-ω-MCA
CDCA
DCA
HDCA
GCA
TCDCA
TDCA
THDCA
UDCA
F
Relative BA-sulfate levels
CA-sulfate
TCA-sulfate
G
Relative BAs levels
CA
TCA
H
Relative Luc activity
Vehicle
Fex
T-βMCA
I
Bile acid
BA-sulfate
Chondrotin
C-sulfate
β-Catenin
TCF/LEF
WNT target gene transcription
TβMCA
TLE3
FXR
C-sulfate treatment

$Apc^{\Delta gut\text{-}Het}Papss2^{\Delta gut}$ mice was confirmed by real-time PCR (Fig. S3D). The unchallenged $Papss2^{\Delta gut}$ mice were healthy and showed no difference in the expression of intestinal stem cell marker genes compared to the floxed controls (Fig. S3E).

Compared with the $Apc^{\Delta gut\text{-}Het}$ controls, $Apc^{\Delta gut\text{-}Het}Papss2^{\Delta gut}$ mice exhibited exacerbated gut tumorigenesis, as evidenced by the gross appearance of the intestine and colon tissues (Fig. 2A), increased total tumor area (Fig. 2B), tumor numbers (Fig. 2C), and the number of large tumors (diameter >2 mm) (Fig. 2D), as well as decreased colon length (Fig. 2E). The sensitization of $Apc^{\Delta gut\text{-}Het}Papss2^{\Delta gut}$ mice was further supported by their higher serum level of carcinoembryonic antigen (CEA) (Fig. 2F), increased inflammation and cancer stemness, as evidenced by increased serum levels of inflammatory cytokines (Fig. 2G), ileal mRNA expression of inflammatory cytokine, macrophage, and intestinal/cancer stem cell marker genes (Fig. 2H). At the histologic level, $Apc^{\Delta gut\text{-}Het}Papss2^{\Delta gut}$ mice showed increased tumor morphology (Fig. 2I) and Ki67 immunostaining (Fig. 2J) in both the ileum and colon.

In another colitis-independent colon cancer model induced by 6-rounds of carcinogen AOM administration as outlined in Fig. 2K[27], the $Papss2^{\Delta gut}$ mice exhibited aggravated colonic tumorigenesis, as evidenced by the gross appearance of the colon tissues (Fig. 2L), increased tumor incidence (Fig. 2M), total tumor area (Fig. 2N) and tumor numbers (Fig. 2O), and decreased colon length (Fig. 2P) and body weight (Fig. 2Q) The exacerbation of AOM-induced gut tumorigenesis was also accompanied by a higher serum level of CEA (Fig. 2R), but inflammation was not affected (Fig. 2S). Increased gut tumorigenesis in AOM-treated $Papss2^{\Delta gut}$ mice was verified histologically by H&E staining and Ki67 immunostaining (Fig. 2T).

### 3.3. *Sensitization of gut tumorigenesis by intestinal Papss2 ablation is accompanied by the activation of Wnt/β-catenin signaling and suppression of Wnt repressor TLE3*

To determine the mechanism by which intestinal ablation of *Papss2* exacerbates gut tumorigenesis, we performed Hallmark pathway analysis on our RNA-seq data derived from intestinal tumors of $Apc^{\Delta gut\text{-}Het}$ and $Apc^{\Delta gut\text{-}Het}Papss2^{\Delta gut}$ mice. Wnt/β-catenin signaling, a well-known colon cancer driver, was one of the top 20 pathways upregulated in $Apc^{\Delta gut\text{-}Het}Papss2^{\Delta gut}$ tumors (Fig. 3A). Gene set enrichment analysis (GSEA) of RNA-seq data showed a robust up-regulation of Wnt/β-catenin signaling and Myc targets in $Apc^{\Delta gut\text{-}Het}Papss2^{\Delta gut}$ tumors (Fig. 3B). Activation of Wnt/β-catenin signaling in $Apc^{\Delta gut\text{-}Het}Papss2^{\Delta gut}$ tumors was further confirmed by their increased mRNA expression of Wnt target genes (Fig. 3C), and protein expression (Fig. 3D) and nuclear translocation (Fig. 3E) of β-catenin. Increased protein expression (Fig. 3F) and nuclear translocation (Fig. 3G) of β-catenin were also observed in AOM-induced $Papss2^{\Delta gut}$ tumors. Transducin-like enhancer of split (TLE3) is a well-established Wnt repressor[28]. $Apc^{\Delta gut\text{-}Het}Papss2^{\Delta gut}$ tumors exhibited decreased protein expression of Tle3 as shown by Western blotting (Fig. 3D) and immunohistochemistry (Fig. 3H). The AOM-induced tumors in $Papss2^{\Delta gut}$ mice also showed decreased protein expression of Tle3 as shown by Western blotting (Fig. 3F), which may have contributed to the activation of Wnt/β-catenin signaling.

In patient samples, the stage-dependent suppression of TLE3 was also found in the human colon cancer tissue arrays by immunohistochemistry (Fig. 3I), and the immunostaining signal of TLE3 showed a positive correlation with the expression of PAPSS2 in the same cohort of patients (Fig. 3J). Gene Expression Profiling Interactive Analysis web server (GEPIA)[29] analyses of the human colon adenocarcinoma patients showed the expression of PAPSS2 has a positive correlation with TLE3 expression (Fig. 3K), but an inverse correlation with the expression of Wnt (Fig. 3L) and β-catenin (Fig. 3M) target genes. The patient results suggested that loss of PAPSS2 led to a decreased expression of TLE3 and activation of Wnt-β-catenin signaling, consistent with the mouse data.

In the human colon cancer HCT116 cells, treatment with the pharmacological PAPSS2 inhibitor $NaClO_3$ activated the transfected Wnt/β-catenin responsive TCF/LEF-Luc report gene[30]. In contrast, in the same TCF/LEF-Luc transfected HCT116 cells, co-transfection of PAPSS2 expression plasmid suppressed the report activity (Fig. 3N). The suppression of β-catenin and induction of TLE3 in PAPSS2 overexpressed HCT116 cells were verified by Western blotting (Fig. 3O).

### 3.4. *Inhibition of Papss2 suppresses intestinal organoid differentiation and activates Wnt/β-catenin signaling*

Stem cell-derived intestinal organoids are composed of a round core of differentiated cells and proliferating outpockets that surround the core, resembling the villus and crypt compartments, respectively[31]. We used intestinal organoids to further characterize the effects of PAPSS2 inhibition on intestinal differentiation and Wnt/β-catenin signaling. Intestinal organoids isolated from $Apc^{\Delta gut\text{-}Het}Papss2^{\Delta gut}$ mice exhibited inhibition of normally balanced growth and differentiation compared to those isolated from $Apc^{\Delta gut\text{-}Het}$ mice, as shown by decreased budding and branching as quantified as crypt domains per organoid and increased proliferation as measured by Ki67 immunostaining (Fig. 4A and Supporting Information Fig. S4A). Treatment of intestinal organoids isolated from $Apc^{\Delta gut\text{-}Het}$ mice with the sulfation inhibitor $NaClO_3$ showed a similar pattern of effect (Fig. 4B and Fig. S4B). GSEA of RNA-seq data showed a robust up-regulation of Wnt/β-catenin signaling and Myc targets in $NaClO_3$-treated $Apc^{\Delta gut\text{-}Het}$ intestinal organoids (Fig. 4C). Activation of Wnt/β-catenin signaling was further confirmed by

**Figure 7** $Apc^{\Delta gut\text{-}Het}Papss2^{\Delta gut}$ mice exhibit disrupted bile acid homeostasis and inhibition of FXR, which may have contributed to Wnt/β-catenin activation. $Apc^{\Delta gut\text{-}Het}$ and $Apc^{\Delta gut\text{-}Het}Papss2^{\Delta gut}$ mice are the same as described in Fig. 2 (A) Serum total bile acids (BAs) levels. (B) Ileal BAs levels. (C) Relative expression of FXR target genes in the ileum. (D, E) 3D PCoA score plot (D) and heatmap (E) of individual ileal BAs profile. (F, G) Relative CA-sulfate and TCA-sulfate levels (F), and parent CA and TCA levels (G) in the ileum measured by UPLC−QTOFMS. $n = 7$ per group. (H) Luciferase reporter assay in HCT116 cells transfected with the TCF/TEF-luciferase reporter and treatment with FXR agonist Fex (50 μmol/L) or antagonist T-β-MCA (50 μmol/L). $n = 4$−5. (I) Schematic summary of the effects of PAPSS2 inhibition on chondroitin sulfation and FXR−TLE3 axis, leading to the activation of Wnt/β-catenin signaling and sensitization of gut tumorigenesis. Statistical significance between two groups was assessed by two-tailed Student's *t*-test. Data are presented as the mean ± SEM or box plots. $^*P < 0.05$; $^{**}P < 0.01$; $^{***}P < 0.001$. The diagram was created with BioRender.

increased expression of Wnt target genes in intestinal organoids isolated from $Apc^{\Delta gut\text{-}Het}Papss2^{\Delta gut}$ mice (Fig. 4D) or $NaClO_3$-treated intestinal organoids isolated from $Apc^{\Delta gut\text{-}Het}$ mice (Fig. 4E). Moreover, treatment of intestinal organoids isolated from $Apc^{\Delta gut\text{-}Het}Papss2^{\Delta gut}$ mice with the Wnt/β-catenin inhibitor cardamonin[32] normalized differentiation and cell proliferation (Fig. 4F and Fig. S4C), suggesting that activation of Wnt/β-catenin signaling was responsible for PAPSS2 deficiency responsive inhibition of intestinal organoid differentiation.

### 3.5. *Intestinal deficiency of Papss2 inhibits chondroitin sulfation, leading to β-catenin activation*

Chondroitin is a sulfation substrate[33]. CS, a widely used dietary supplement to treat osteoarthritis, was suggested to inhibit CRC based on some experimental and epidemiological evidence, but without a defined mechanism[34,35]. As expected, and as a result of sulfation inhibition, the content of CS was markedly reduced in the intestine and colon of tumor-bearing $Apc^{\Delta gut\text{-}Het}Papss2^{\Delta gut}$ mice (Fig. 5A and B) and AOM-treated $Papss2^{\Delta gut}$ mice (Fig. 5C and D), as shown by immunofluorescence (Fig. 5A and C) and Western blotting (Fig. 5B and D), respectively. The lack of complete inhibition of chondroitin sulfation may have been accounted for by the intact expression of Papss1 in $Papss2^{\Delta gut}$ mice[15]. The decrease of CS in $Apc^{\Delta gut\text{-}Het}Papss2^{\Delta gut}$ mice was functionally relevant, because treatment of intestinal organoids with CS rescued *Papss2* deficiency-responsive inhibition of differentiation and induction of cell proliferation (Fig. 5E). CS has been reported as a negative regulator of Wnt/β-catenin in breast cancer cells[36]. We also found that CS treatment inhibited the TCF/LEF-Luc reporter activity in HCT116 cells (Fig. 5F) and inhibited β-catenin expression in intestinal organoids isolated from $Apc^{\Delta gut\text{-}Het}Papss2^{\Delta gut}$ mice and AOM-treated $Papss2^{\Delta gut}$ mice (Fig. 5G).

### 3.6. *Chondroitin sulfate supplementation attenuates gut tumorigenesis in* $Apc^{\Delta gut\text{-}Het}Papss2^{\Delta gut}$ *mice*

To determine whether CS protected mice from gut tumorigenesis *in vivo*, we treated $Apc^{\Delta gut\text{-}Het}$ or $Apc^{\Delta gut\text{-}Het}Papss2^{\Delta gut}$ mice with CS (400 mg/kg daily oral gavage). While CS had little effect on the tumorigenesis of $Apc^{\Delta gut\text{-}Het}$ mice, CS supplementation markedly attenuated *Papss2* deficiency-induced gut tumorigenesis, as evidenced by the gross appearance of the intestine and colon tissues (Fig. 6A), as well as decreased total tumor area (Fig. 6B), tumor numbers (Fig. 6C), the number of large tumors (diameter >2 mm) (Fig. 6D), and normalization of colon length (Fig. 6E). At the histological level, increased tumor morphology (Fig. 6F) and Ki67 immunostaining (Fig. 6G) observed in $Apc^{\Delta gut\text{-}Het}Papss2^{\Delta gut}$ mice were attenuated upon the CS treatment. As expected, treatment of $Apc^{\Delta gut\text{-}Het}Papss2^{\Delta gut}$ mice with CS recovered the CS level in the gut (Fig. 6H), inhibited nuclear translocation of β-catenin (Fig. 6I), and decreased the mRNA expression of Wnt target genes and inflammatory marker genes (Fig. 6J).

### 3.7. $Apc^{\Delta gut\text{-}Het}Papss2^{\Delta gut}$ *mice exhibit disrupted bile acid homeostasis and inhibition of FXR, which may have contributed to Wnt/β-catenin activation*

Bile acids are common substrates of sulfation, and sulfoconjugation controls bile acid homeostasis by impacting bile acid elimination and detoxification[37]. Meanwhile, activation of the bile acid sensing nuclear receptor FXR has been shown to inhibit gut tumorigenesis[38–40]. Compared to $Apc^{\Delta gut\text{-}Het}$ mice, $Apc^{\Delta gut\text{-}Het}Papss2^{\Delta gut}$ mice showed increased levels of total bile acids in the serum (Fig. 7A) and ileum (Fig. 7B). But to our surprise, the ileal mRNA expression of FXR target genes, including fibroblast growth factor 15 (*Fgf15*), small heterodimer partner (*Shp*), and ileal bile acid-binding protein (*Ibabp*), was markedly decreased in $Apc^{\Delta gut\text{-}Het}Papss2^{\Delta gut}$ mice (Fig. 7C). Metabolomic profiling showed the ileum levels of several FXR antagonistic bile acid species, including T-α-MCA and T-β-MCA, were elevated in $Apc^{\Delta gut\text{-}Het}Papss2^{\Delta gut}$ mice as shown by 3D PCoA score plot (Fig. 7D) and heatmap (Fig. 7E), which may have explained the inhibition of FXR activity. We further measured the levels of sulfonated bile acids and their patent species and found the ileum levels of CA-sulfate and TCA-sulfate were decreased (Fig. 7F), whereas the levels of the parent CA and TCA were increased (Fig. 7G) in $Apc^{\Delta gut\text{-}Het}Papss2^{\Delta gut}$ mice. CS supplementation did not affect the total bile acid levels in the serum (Supporting Information Fig. S5A) and ileum (Fig. S5B) of $Apc^{\Delta gut\text{-}Het}$ and $Apc^{\Delta gut\text{-}Het}Papss2^{\Delta gut}$ mice. In HCT116 cells transfected with GAL4-hFXR LBD and the GAL4-responsive luciferase report tk-UAS-Luc, neither CA nor CA-sulfate was effective in activating FXR, whereas both TCA and TCA-sulfate induced the reporter gene activity with a similar potency (Supporting Information Fig. S6).

FXR has recently been reported to suppress colorectal cancer by inhibiting the Wnt/β-catenin pathway *via* the transcriptional activation of the Wnt repressor TLE3[28]. The inhibition FXR activity provided a plausible mechanism by which *Papss2* ablation suppressed TLE3 (Fig. 3) and activated Wnt/β-catenin signaling. Consistent with the notion that activation of FXR inhibits Wnt/β-catenin, we showed that treatment of HCT116 cells with the FXR agonist fexaramine (Fex) and FXR antagonist T-β-MCA inhibited and activated the TCF/LEF-Luc reporter activity, respectively (Fig. 7H). As summarized in Fig. 7I, our results demonstrated that both the inhibition of chondroitin sulfation and accumulation of FXR antagonizing bile acids as results of Papss2 ablation contributed to the activation of Wnt/β-catenin signaling and exacerbation of gut tumorigenesis in $Apc^{\Delta gut\text{-}Het}Papss2^{\Delta gut}$ mice.

## 4. Discussion

Our study reveals that intestinal ablation of PAPSS2 sensitizes mice to APC deficiency-induced gut tumorigenesis through the activation of Wnt/β-catenin signaling. We propose that the expression of PAPSS2 is protective in colon cancer through PAPSS2-mediated chondroitin sulfation and activation of the FXR-TLE3 axis, leading to the inhibition of Wnt/β-catenin signaling pathway.

Wnt/β-catenin signaling is often associated with cell proliferation, cell polarity, developmental cell-fate determination, tissue homeostasis, and cancers[41–43]. Wnt/β-catenin is aberrantly activated in most CRC through the loss of function mutations of the tumor suppressor APC[44,45]. The notion that Wnt/β-catenin is activated when there is a loss of function of APC led to our hypothesis that the sensitization of $Apc^{\Delta gut\text{-}Het}Papss2^{\Delta gut}$ mice to gut tumorigenesis may have resulted from exacerbated activation of Wnt/β-catenin. Indeed, RNA-seq analysis of the $Apc^{\Delta gut\text{-}Het}Papss2^{\Delta gut}$ tumors and intestinal organoids showed that Wnt/β-catenin signaling was markedly upregulated. We went on

to show that activation of Wnt/β-catenin was required for the sensitization, because treatment of intestinal organoids isolated from $Apc^{\Delta gut\text{-}Het}Papss2^{\Delta gut}$ mice with the Wnt/β-catenin inhibitor cardamonin normalized differentiation.

The mechanism by which Papss2 inhibition activates Wnt/β-catenin and sensitizes gut tumorigenesis was intriguing. Knowing the inhibition of protein sulfation, such as that of p53, had pathophysiological consequence[26], we initiated hypothesized the β-catenin or Wnt ligands might be sulfation substrates, but our preliminary results suggested otherwise. Our further mechanistic characterizations suggested that the activation of Wnt/β-catenin in $Apc^{\Delta gut\text{-}Het}Papss2^{\Delta gut}$ mice was likely accounted for by the combined effect of loss of CS and accumulation of FXR antagonistic bile acid species as a result of loss of sulfation. CS is a key component of the extracellular matrix (ECM), which provides structural support to cells. The Wnt/β-catenin pathway is closely linked to cell adhesion and signaling within the ECM. Changes in the ECM, including alterations in CS content, can affect the Wnt signaling cascade. The notion that decreased CS levels may have contributed to Wnt/β-catenin activation was consistent with the report that CS is a negative regulator of the Wnt/β-catenin pathway in breast cancer cells[36]. Moreover, we showed that supplementation of CS in intestinal organoids or *in vivo* was effective in attenuating the effect of Papss2 ablation on organoid differentiation and gut tumorigenesis. Sulfation of bile acids is a major pathway for bile acid elimination and detoxification[37]. The PAPSS2 is the key enzyme to synthesize PAPS, which is the universal sulfonate donor for all sulfations, including the sulfation of bile acids. We found the sulfation of CA, and TCA was decreased, and the levels of parent CA, and TCA were increased, in the ileum $Apc^{\Delta gut\text{-}Het}Papss2^{\Delta gut}$ mice. The accumulation of FXR antagonistic bile acid species, such as T-β-MCA, and inhibition of FXR activity in $Apc^{\Delta gut\text{-}Het}Papss2^{\Delta gut}$ mice was consistent with our previous findings in colitis-promoted colonic carcinogenesis[16], but the current study revealed novel mechanistic insight. We believe the inhibition of FXR contributed to Wnt/β-catenin activation in $Apc^{\Delta gut\text{-}Het}Papss2^{\Delta gut}$ mice, because the FXR-TLE3 gene regulatory axis has been reported to negatively regulate Wnt/β-catenin activity. The expression of TLE3, a Wnt suppressor and FXR target gene, was decreased in the mouse and human colon cancer, likely as a result of inhibition of FXR activity. In addition to activating Wnt/β-catenin, inhibition of FXR can also lead to the activation of NF-κB signaling pathways[46]. Indeed, increased inflammation was observed in the tumor-bearing $Apc^{\Delta gut\text{-}Het}Papss2^{\Delta gut}$ mice (data not shown), which may have also contributed to increased gut tumorigenesis.

Our results are of high clinical relevance. A decreased expression of PAPSS2 in human colon tumors was verified by immunohistochemistry analysis of human colon cancer tissue arrays. Our bioinformatic analysis showed PAPSS2 is an accurate marker to distinguish COAD patients by ROC analysis, and the decreased expression of PAPSS2 correlates with poor colon cancer patient survival. Moreover, we found that the expression of PAPSS2 positively correlated with the expression of TLE3, and negatively correlated with the expression of Wnt/β-catenin target genes in COAD patients. Besides COAD, a lower expression of PAPSS2 was correlated with poorer survival in four other cancer types, including head and neck squamous cell carcinoma (HNSC), pancreatic adenocarcinoma (PAAD), kidney renal clear cell carcinoma (KIRC), and lung adenocarcinoma (LUAD). Future studies are necessary to determine whether and how PAPSS2 plays a role in the pathogenesis of these cancer types.

Our mechanistic defining of chondroitin sulfate as an anti-colon cancer agent is also highly translational. Chondroitin sulfate has long been used as a dietary supplement against osteoarthritis. It has also been used as an antioxidant, antitumor, anticoagulant, and immune-regulatory agent, or as biomaterial scaffolds in tissue engineering and drug delivery[47]. Oral supplementation of CS is well-tolerated by humans with favorable pharmacokinetics. Although CS has shown some beneficial effects to suppress colon cancer cell growth *in vitro*[48–50], the molecular mechanism was not defined. Here, we found CS treatment *in vitro* or *in vivo* attenuated *Papss2* deficiency-induced and APC deficiency-responsive gut tumorigenesis through the inhibition of Wnt/β-catenin signaling pathway. Science CS treatment had little effect on tumor regression in APC deficiency mice, it is possible that CS may not play a key role in tumor initiation, but it may be critical in restricting tumor progression when *Papss2* is lacking. Colonic carcinogenesis can also be influenced by the gut microbiome, we cannot exclude the possibility that changes in gut microbiome may have also contributed to the phenotypic exhibition in our $Apc^{\Delta gut\text{-}Het}Papss2^{\Delta gut}$ mice.

## 5. Conclusions

We have uncovered that PAPSS2-mediated chondroitin sulfation and PAPSS2-bile acids−FXR−TLE3−WNT/β-catenin axis play an essential role in *Papss2* deficiency-responsive gut tumorigenesis. We propose that intestinal PAPSS2 or sulfation represent a potential therapeutic target for colon cancer and CS may be explored for its use in the prevention and treatment of colon cancer.

## Acknowledgments

This work was supported by NIH grants DK117370, DK135538, and ES030429 (to Wen Xie, US) and a Pilot & Feasibility grant (to Pengfei Xu, US) from the Pittsburgh Liver Research Center funded by NIH grant P30DK120531. Authors would like to acknowledge NIH shared instrumentation grant: Olympus FV3000 Confocal Microscope SIG: NIH S10OD030254-01A1.

## Author contributions

Wen Xie conceived and mentored this research. Wen Xie and Pengfei Xu designed the study. Pengfei Xu, Yue Xi, Jong-Won Kim, Junjie Zhu, and Min Zhang performed the experiments and analyzed the data. Meishu Xu, Songrong Ren, Da Yang, and Xiaochao Ma gave technical support and conceptual advice. Pengfei Xu and Wen Xie wrote the manuscript. All authors reviewed and approved the final manuscript.

## Conflicts of interest

The authors declare no conflicts of interest.

## Appendix A. Supporting information

Supporting data to this article can be found online at https://doi.org/10.1016/j.apsb.2023.12.006.

## References


1. Arnold M, Abnet CC, Neale RE, Vignat J, Giovannucci EL, McGlynn KA, et al. Global burden of 5 major types of gastrointestinal cancer. *Gastroenterology* 2020;**159**:335−49.e15.
2. Xi Y, Xu P. Global colorectal cancer burden in 2020 and projections to 2040. *Transl Oncol* 2021;**14**:101174.
3. Li C, Wang Y, Liu D, Wong CC, Coker OO, Zhang X, et al. Squalene epoxidase drives cancer cell proliferation and promotes gut dysbiosis to accelerate colorectal carcinogenesis. *Gut* 2022;**71**:2253−65.
4. Crockett SD, Nagtegaal ID. Terminology, molecular features, epidemiology, and management of serrated colorectal neoplasia. *Gastroenterology* 2019;**157**:949−66.e4.
5. Wang S, Qu Y, Xia P, Chen Y, Zhu X, Zhang J, et al. Transdifferentiation of tumor infiltrating innate lymphoid cells during progression of colorectal cancer. *Cell Res* 2020;**30**:610−22.
6. Olkinuora AP, Peltomaki PT, Aaltonen LA, Rajamaki K. From APC to the genetics of hereditary and familial colon cancer syndromes. *Hum Mol Genet* 2021;**30**:R206−24.
7. Sun L, Wan A, Zhou Z, Chen D, Liang H, Liu C, et al. RNA-binding protein RALY reprogrammes mitochondrial metabolism *via* mediating miRNA processing in colorectal cancer. *Gut* 2021;**70**:1698−712.
8. Gao J, Wu Z, Zhao M, Zhang R, Li M, Sun D, et al. Allosteric inhibition reveals SHP2-mediated tumor immunosuppression in colon cancer by single-cell transcriptomics. *Acta Pharm Sin B* 2022;**12**:149−66.
9. Liu H, Huang Q, Fan Y, Li B, Liu X, Hu C. Dissecting the novel abilities of aripiprazole: the generation of anti-colorectal cancer effects by targeting Galphaq *via* HTR2B. *Acta Pharm Sin B* 2023;**13**:3400−13.
10. Lahde M, Heino S, Hogstrom J, Kaijalainen S, Anisimov A, Flanagan D, et al. Expression of R-spondin 1 in $Apc^{Min/+}$ mice suppresses growth of intestinal adenomas by altering Wnt and transforming growth factor beta signaling. *Gastroenterology* 2021;**160**:245−59.
11. Ren J, Sui H, Fang F, Li Q, Li B. The application of $Apc^{Min/+}$ mouse model in colorectal tumor researches. *J Cancer Res Clin Oncol* 2019;**145**:1111−22.
12. Bugter JM, Fenderico N, Maurice MM. Mutations and mechanisms of WNT pathway tumour suppressors in cancer. *Nat Rev Cancer* 2021;**21**:5−21.
13. Sun L, Zhang Y, Cai J, Rimal B, Rocha ER, Coleman JP, et al. Bile salt hydrolase in non-enterotoxigenic bacteroides potentiates colorectal cancer. *Nat Commun* 2023;**14**:755.
14. Cook DR, Kang M, Martin TD, Galanko JA, Loeza GH, Trembath DG, et al. Aberrant expression and subcellular localization of ECT2 drives colorectal cancer progression and growth. *Cancer Res* 2022;**82**:90−104.
15. Xu P, Cai X, Guan X, Xie W. Sulfoconjugation of protein peptides and glycoproteins in physiology and diseases. *Pharmacol Ther* 2023;**251**:108540.
16. Xu P, Xi Y, Zhu J, Zhang M, Luka Z, Stolz DB, et al. Intestinal sulfation is essential to protect against colitis and colonic carcinogenesis. *Gastroenterology* 2021;**161**:271−86.e11.
17. Bai X, Wei H, Liu W, Coker OO, Gou H, Liu C, et al. Cigarette smoke promotes colorectal cancer through modulation of gut microbiota and related metabolites. *Gut* 2022;**71**:2439−50.
18. Xu P, Wang J, Hong F, Wang S, Jin X, Xue T, et al. Melatonin prevents obesity through modulation of gut microbiota in mice. *J Pineal Res* 2017;**62**:e12399.
19. Shi J, Ju R, Gao H, Huang Y, Guo L, Zhang D. Targeting glutamine utilization to block metabolic adaptation of tumor cells under the stress of carboxyamidotriazole-induced nutrients unavailability. *Acta Pharm Sin B* 2022;**12**:759−73.
20. Xi Y, Li Y, Xu P, Li S, Liu Z, Tung HC, et al. The anti-fibrotic drug pirfenidone inhibits liver fibrosis by targeting the small oxidoreductase glutaredoxin-1. *Sci Adv* 2021;**7**:eabg9241.
21. Jiang C, Xie C, Li F, Zhang L, Nichols RG, Krausz KW, et al. Intestinal farnesoid X receptor signaling promotes nonalcoholic fatty liver disease. *J Clin Invest* 2015;**125**:386−402.
22. Zhu J, Wang P, Shehu AI, Lu J, Bi H, Ma X. Identification of novel pathways in idelalisib metabolism and bioactivation. *Chem Res Toxicol* 2018;**31**:548−55.
23. Yan J, Tung HC, Li S, Niu Y, Garbacz WG, Lu P, et al. Aryl hydrocarbon receptor signaling prevents activation of hepatic stellate cells and liver fibrogenesis in mice. *Gastroenterology* 2019;**157**:793−806.
24. Uhlen M, Fagerberg L, Hallstrom BM, Lindskog C, Oksvold P, Mardinoglu A, et al. Proteomics. Tissue-based map of the human proteome. *Science* 2015;**347**:1260419.
25. Karlsson M, Zhang C, Mear L, Zhong W, Digre A, Katona B, et al. A single-cell type transcriptomics map of human tissues. *Sci Adv* 2021;**7**:eabh2169.
26. Xu P, Xi Y, Wang P, Luka Z, Xu M, Tung HC, et al. Inhibition of p53 sulfoconjugation prevents oxidative hepatotoxicity and acute liver failure. *Gastroenterology* 2022;**162**:1226−41.
27. Luo Y, Xie C, Brocker CN, Fan J, Wu X, Feng L, et al. Intestinal PPAR$\alpha$ protects against colon carcinogenesis *via* regulation of methyltransferases DNMT1 and PRMT6. *Gastroenterology* 2019;**157**:744−59.e4.
28. Dong X, Cai C, Fu T. FXR suppresses colorectal cancer by inhibiting the Wnt/$\beta$-catenin pathway *via* activation of TLE3. *Genes Dis* 2022;**10**:719−22.
29. Tang Z, Li C, Kang B, Gao G, Li C, Zhang Z. GEPIA: a web server for cancer and normal gene expression profiling and interactive analyses. *Nucleic Acids Res* 2017;**45**:W98−102.
30. Schuijers J, Mokry M, Hatzis P, Cuppen E, Clevers H. Wnt-induced transcriptional activation is exclusively mediated by TCF/LEF. *EMBO J* 2014;**33**:146−56.
31. Kadosh E, Snir-Alkalay I, Venkatachalam A, May S, Lasry A, Elyada E, et al. The gut microbiome switches mutant p53 from tumour-suppressive to oncogenic. *Nature* 2020;**586**:133−8.
32. Shrivastava S, Jeengar MK, Thummuri D, Koval A, Katanaev VL, Marepally S, et al. Cardamonin, a chalcone, inhibits human triple negative breast cancer cell invasiveness by downregulation of Wnt/beta-catenin signaling cascades and reversal of epithelial−mesenchymal transition. *Biofactors* 2017;**43**:152−69.
33. Cortes M, Baria AT, Schwartz NB. Sulfation of chondroitin sulfate proteoglycans is necessary for proper Indian hedgehog signaling in the developing growth plate. *Development* 2009;**136**:1697−706.
34. Zhou Y, Li X, Morita Y, Hachimura S, Miyakawa T, Takahashi S, et al. Identification of the effects of chondroitin sulfate on inhibiting CDKs in colorectal cancer based on bioinformatic analysis and experimental validation. *Front Oncol* 2021;**11**:705939.
35. Kantor ED, Zhang X, Wu K, Signorello LB, Chan AT, Fuchs CS, et al. Use of glucosamine and chondroitin supplements in relation to risk of colorectal cancer: results from the Nurses' health study and health professionals follow-up study. *Int J Cancer* 2016;**139**:1949−57.
36. Willis CM, Kluppel M. Chondroitin sulfate-E is a negative regulator of a pro-tumorigenic Wnt/beta-catenin−collagen 1 axis in breast cancer cells. *PLoS One* 2014;**9**:e103966.
37. Alnouti Y. Bile acid sulfation: a pathway of bile acid elimination and detoxification. *Toxicol Sci* 2009;**108**:225−46.
38. Tang Q, Evans RM. Colon cancer checks in when bile acids check out: the bile acid-nuclear receptor axis in colon cancer. *Essays Biochem* 2021;**65**:1015−24.
39. Bailey AM, Zhan L, Maru D, Shureiqi I, Pickering CR, Kiriakova G, et al. FXR silencing in human colon cancer by DNA methylation and KRAS signaling. *Am J Physiol Gastrointest Liver Physiol* 2014;**306**:G48−58.

40. Xu P. Nuclear receptors in health and diseases. *Int J Mol Sci* 2023;**24**:9153.
41. Carotenuto P, Fassan M, Pandolfo R, Lampis A, Vicentini C, Cascione L, et al. Wnt signalling modulates transcribed-ultraconserved regions in hepatobiliary cancers. *Gut* 2017;**66**:1268−77.
42. Tian W, Li J, Wang Z, Zhang T, Han Y, Liu Y, et al. HYD-PEP06 suppresses hepatocellular carcinoma metastasis, epithelial−mesenchymal transition and cancer stem cell-like properties by inhibiting PI3K/AKT and WNT/beta-catenin signaling activation. *Acta Pharm Sin B* 2021;**11**:1592−606.
43. Braeuning A, Schwarz M. Regulation of expression of drug-metabolizing enzymes by oncogenic signaling pathways in liver tumors: a review. *Acta Pharm Sin B* 2020;**10**:113−22.
44. Perugorria MJ, Olaizola P, Labiano I, Esparza-Baquer A, Marzioni M, Marin JJG, et al. Wnt−beta-catenin signalling in liver development, health and disease. *Nat Rev Gastroenterol Hepatol* 2019;**16**:121−36.
45. Sferrazza G, Corti M, Brusotti G, Pierimarchi P, Temporini C, Serafino A, et al. Nature-derived compounds modulating Wnt/beta-catenin pathway: a preventive and therapeutic opportunity in neoplastic diseases. *Acta Pharm Sin B* 2020;**10**:1814−34.
46. Fu T, Coulter S, Yoshihara E, Oh TG, Fang S, Cayabyab F, et al. FXR regulates intestinal cancer stem cell proliferation. *Cell* 2019;**176**:1098−112.e18.
47. Restaino OF, Schiraldi C. Chondroitin sulfate: are the purity and the structural features well assessed? A review on the analytical challenges. *Carbohydr Polym* 2022;**292**:119690.
48. Wu R, Shen Q, Li G, Li P, Shang N. The regulatory network of sturgeon chondroitin sulfate on colorectal cancer inhibition by transcriptomic and proteomic analysis. *Int J Mol Sci* 2021;**22**:9395.
49. Wu R, Shen Q, Li P, Shang N. Sturgeon chondroitin sulfate restores the balance of gut microbiota in colorectal cancer bearing mice. *Int J Mol Sci* 2022;**23**:3723.
50. Wu R, Shang N, Gui M, Yin J, Li P. Sturgeon (Acipenser)-derived chondroitin sulfate suppresses human colon cancer HCT-116 both *in vitro* and *in vivo* by inhibiting proliferation and inducing apoptosis. *Nutrients* 2020;**12**:1130.